frontiers | Frontiers in Materials

TYPE Original Research
PUBLISHED 17 November 2022
DOI 10.3389/fmats.2022.1052261

OPEN ACCESS

EDITED BY
Nitish Bibhanshu,
Ames Laboratory, United States

REVIEWED BY
Sumit Ghosh,
University of Oulu, Finland
Jesus Porcayo-Calderon,
Universidad Autónoma del Estado de Morelos, Mexico

*CORRESPONDENCE
David M. Bastidas,
dbastidas@uakron.edu

SPECIALTY SECTION
This article was submitted to Structural Materials,
a section of the journal
Frontiers in Materials

RECEIVED 23 September 2022
ACCEPTED 03 November 2022
PUBLISHED 17 November 2022

CITATION
Ress J, Martin U and Bastidas DM (2022), Oxygen scavenging activity of smart colophony microcapsules containing nitrite corrosion inhibitors for steel reinforced concrete.
Front. Mater. 9:1052261.
doi: 10.3389/fmats.2022.1052261

Oxygen scavenging activity of smart colophony microcapsules containing nitrite corrosion inhibitors for steel reinforced concrete

Jacob Ress, Ulises Martin and David M. Bastidas*

National Center for Education and Research on Corrosion and Materials Performance, NCERCAMP-UA, Department Chemical, Biomolecular, and Corrosion Engineering, The University of Akron, Akron, OH, United States

In this study, the electrochemical performance of microcapsules (MCs) containing $NaNO_2$ corrosion inhibitors for steel reinforcements was studied in 0.6 M chloride contaminated simulated concrete pore solutions (SCPS) with varying pH for a period of 28 days. The corrosion inhibition was studied by potentiodynamic polarization and electrochemical impedance spectroscopy (EIS). The polarization results for the MC samples showed improved corrosion resistance, with an i_{corr} of 2.54 $\times 10^{-6}$ A/cm^2 after 28 days exposure in SCPS. Oxygen scavenging activity from the MCs was observed by reduced cathodic kinetics, displaying decreased cathodic exchange current densities of 2.66 $\times 10^{-8}$ A/cm^2, thus imparting cathodic inhibition in conjunction with anodic corrosion inhibitors. The microcapsules additionally displayed improvement over free $NaNO_2$ inhibitors after sufficient release time. The decrease in cathodic and anodic kinetics, along with the improved corrosion resistance, show a dual synergistic corrosion inhibition of the $NaNO_2$ loaded colophony MC.

KEYWORDS

smart corrosion inhibitors, microcapsules, chlorides, reinforcements, carbonation, electrochemical impedance spectroscopy

Introduction

Reinforced concrete structures are widely used in global construction industry due to their high mechanical performance, however the corrosion of the reinforcements by aggressive environments lead to deterioration, spalling, loss of integrity, and eventual catastrophic failure (Bazant, 1979; Sánchez-Deza et al., 2018; Zheng et al., 2020). The alkaline concrete environment favors the development of a stable passive film, which impart protection to the reinforcement surface (Macdonald et al., 2020). Concrete reinforcements, however, are susceptible to environmental degradation that can lead to corrosion of the structure (Bastidas et al., 2008; Cao et al., 2022). The major

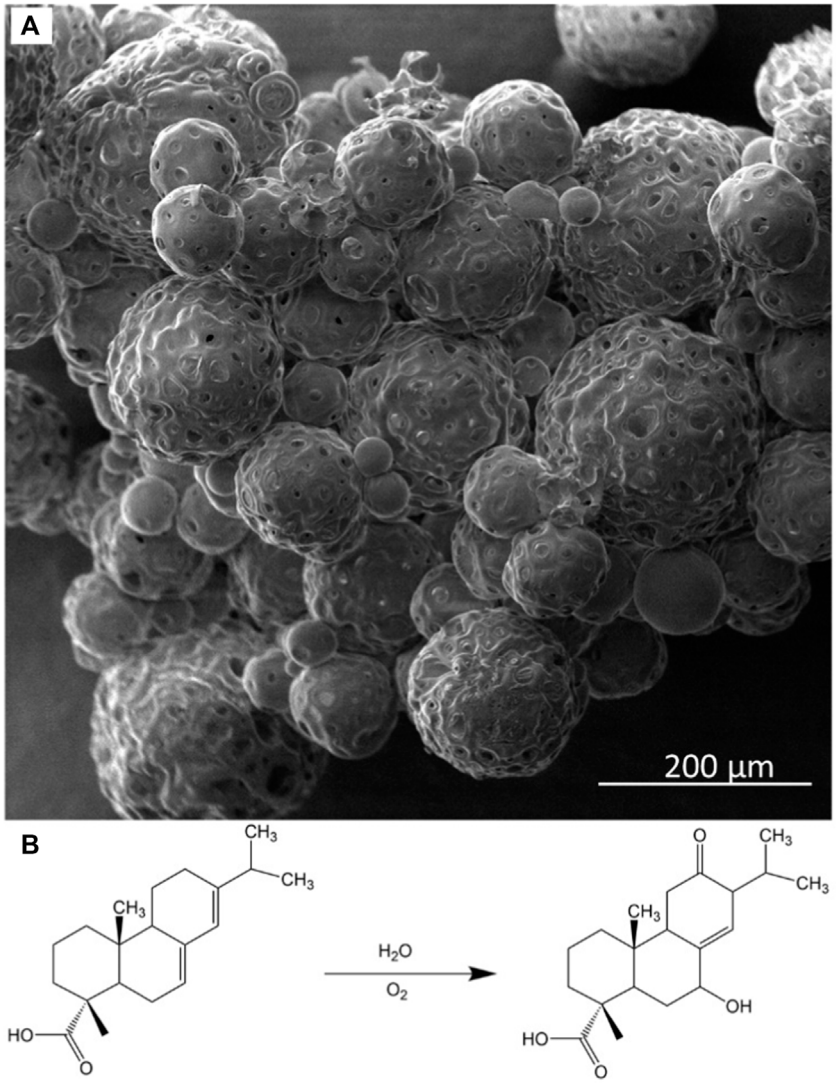

FIGURE 1
(A) SEM image of colophony microcapsules containing $NaNO_2$ corrosion inhibitors and **(B)** oxidation scheme for colophony (abietic acid).

forms of corrosion for rebars used in reinforced concrete are caused by chloride ingress and carbonation, both of which initiate the formation of unstable ferrous oxides (Bastidas et al., 2020; Al-Ameeri et al., 2021). Once chloride ions reach the steel surface and achieve the critical chloride concentration threshold, acid hydrolysis occurs at anodic sites of the reinforcement, initiating pitting corrosion (Kenny and Katz, 2020). Conversely, during the processes of carbonation, atmospheric CO_2 in contact with the concrete matrix reacts to form carbonates and bicarbonates, decreasing the pH of the concrete pore solution from around 12.6 to values near 9 (Andrade, 2020). Moreover, corrosion of the steel reinforcements causes the formation of unstable iron oxyhydroxides at the rebar-concrete interface, conferring increased pressure on the concrete cover, leading to cracking and catastrophic damage to the structure (Bastidas et al., 2020).

Encapsulation provides protection from the loss of corrosion inhibitors due to leaching and premature binding to the admixture in addition to controlled release mechanisms (Calegari et al., 2020). Encapsulation by emulsion *via* water-in-oil-in-water (W/O/W) double emulsion is an effective method due to its relative scalability and low cost (Ding et al., 2019). In the cement and concrete industry, microencapsulation presents an effective way to deliver corrosion inhibitors (Du et al., 2020). Microcapsules can be

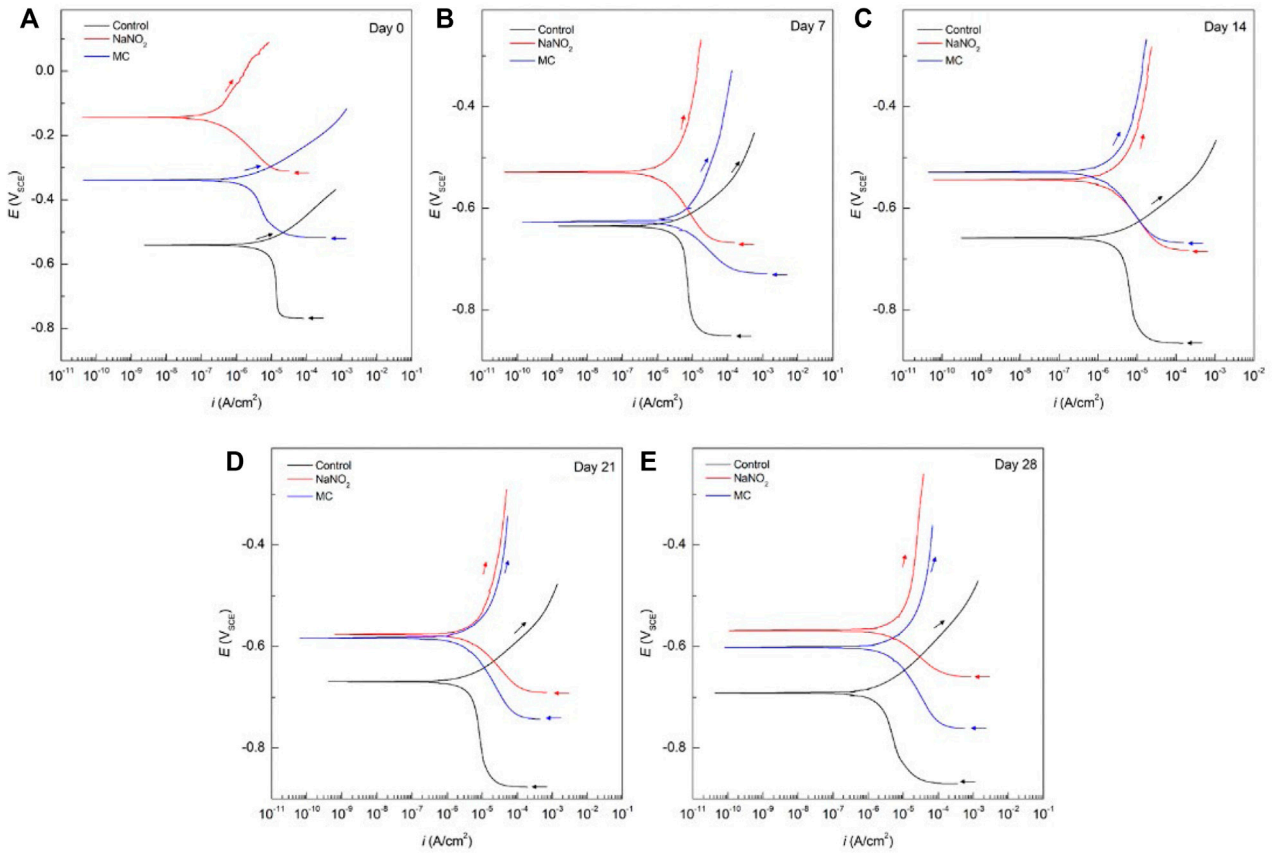

FIGURE 2
Potentiodynamic polarization curves obtained for carbon steel rebars immersed in DI with 0.6 M NaCl for the control sample, free $NaNO_2$ corrosion inhibitor sample, and colophony MCs samples after different time exposure: **(A)** 0 days, **(B)** 7 days, **(C)** 14 days, **(D)** 21 days, and **(E)** 28 days.

synthesized with smart materials to allow for a controlled release with a variety of triggering stimuli such as ionic interactions, temperature, and pH changes (Matsuda et al., 2019; Pan et al., 2022; Zhang et al., 2022). Smart corrosion inhibition can be especially helpful, as losses of corrosion inhibitors is minimized by selective release (Giuliani et al., 2020). Colophony microcapsules containing $NaNO_2$ corrosion inhibitors were previously developed by the authors, studying the physical characteristics and release properties (Ress et al., 2020). These microcapsules utilize a colophony shell due to its compatibility with concrete, enhancement of concrete's mechanical properties, encapsulation capacity, and ability to control release (Cánovas et al., 1989; Panda et al., 2013).

Colophony is primarily composed of abietic acid along with its derivatives and other terpenes (Nong et al., 2013). The colophony microcapsules with alkaline release will allow for mitigation of corrosion inhibitor loss during the concrete mixing stage, due to leaching and premature reaction with the binder by controlling the diffusion of the inhibitors, allowing release once the concrete cures to a highly alkaline pH (~12.6) (P. Kumar Mehta and Paulo J. M. Monteiro, 2014). Additionally, abietic is similar to tannins, which have been shown to decrease dissolved oxygen, in aqueous environments, thus acting as an oxygen scavenger (Scrivenand and Winter 1978).

Oxygen scavengers are molecules that readily oxidize or react with oxygen, thus reducing the availability of oxygen molecules to participate in the cathodic half reaction of the corrosion process. The use of oxygen scavengers to reduce corrosion has been present in industry in the application of boilers, pipelines, *etc.* (Lakshmi Priya et al., 2005). The use of sulfites removes dissolved oxygen by replacing the cathodic reaction of the corrosion process with oxidation of the sulfite into sulfate, thus reducing available oxygen (Rashid and Khadom, 2020). Similarly, organic molecules with alcohol functional groups react with dissolved oxygen, replacing the cathodic reaction of the corrosion process in

TABLE 1 Corrosion potential (E_{corr}) and corrosion current density (i_{corr}) values obtained from carbon steel rebar polarized in deionized water (DI) and simulated concrete pore solution (SCPS) contaminated with 0.6 M NaCl.

Days	Control		$NaNO_2$		MC	
	DI	SCPS	DI	SCPS	DI	SCPS
			E_{corr} (mV_{SCE})			
0	−540	−420	−144	−254	−468	−399
7	−636	−572	−529	−502	−617	−554
14	−658	−607	−577	−522	−620	−539
21	−679	−651	−605	−535	−629	−544
28	−691	−671	−612	−548	−622	−552
			i_{corr} (A/cm^2)			
0	8.29×10^{-6}	8.26×10^{-7}	6.12×10^{-7}	2.10×10^{-7}	4.21×10^{-6}	3.30×10^{-7}
7	5.44×10^{-6}	2.59×10^{-6}	2.86×10^{-6}	1.85×10^{-6}	5.47×10^{-6}	2.28×10^{-6}
14	5.07×10^{-6}	5.16×10^{-6}	2.52×10^{-6}	2.85×10^{-6}	4.02×10^{-6}	1.49×10^{-6}
21	8.12×10^{-6}	6.44×10^{-6}	3.08×10^{-6}	4.76×10^{-6}	5.00×10^{-6}	1.73×10^{-6}
28	9.31×10^{-6}	8.43×10^{-6}	4.24×10^{-6}	5.96×10^{-6}	5.22×10^{-6}	2.54×10^{-6}
			IE (%)			
0	–	–	93	75	73	60
7	–	–	47	29	42	51
14	–	–	50	45	18	71
21	–	–	62	26	38	73
28	–	–	54	29	47	71

favor of oxidation into ketone (Jafar and Fathi, 2015). The use of hydrazine also reacts in place of the metal, forming nitrogen gas (Schremp et al., 1961) Henna extract is made up of aromatic organic compounds, similar to colophony. The main lawsone constituent showed viability as a mixed inhibitor as well as cathodic inhibition *via* oxygen scavenging through the formation of Fe complexes (Ostovari et al., 2009).

In this study, pH triggered colophony microcapsules are used to deliver $NaNO_2$ corrosion inhibitors in simulated concrete pore solution (saturated calcium hydroxide, SCPS) and deionized water (DI) contaminated with 0.6 M NaCl. The anticorrosion performance of smart microcapsules with pH triggered release was studied over the course of 28 days in both test solutions with the presence of chloride ions. Both AC and DC methods were used, electrochemical impedance spectroscopy (EIS) and potentiodynamic polarization (PDP), respectively. The influence of the pH of the chloride containing solutions as well as the synergistic inhibition effect of the colophony based microcapsules were analyzed by studying the electrochemical reaction kinetic parameters of corrosion current density and cathodic exchange current density. The resistances of the passive film and the electrochemical double layer as well as their respective capacitance values were also analyzed to corroborate the DC results and study the changes in the electrode/electrolyte interfaces of the system.

Experimental

Colophony microcapsules (MCs) containing $NaNO_2$ corrosion inhibitors were prepared using the water-in-oil-in-water double emulsion protocol discussed in previous work by authors (Ress et al., 2020). A double emulsion synthetic route was used, in which colophony (Beantown Chemical) was dissolved using diethyl ether (99% Sigma Aldrich) and mixed with an overhead mechanical stirrer. Then, an aqueous solution of $NaNO_2$ and poly-vinyl alcohol (PVA, 99% hydrolized) was added dropwise while stirring to form the first emulsion for 5 min. The second emulsion was formed by the dropwise addition of a solution of PVA as a stabilizing agent to maintain the microcapsule structure before finally evaporating the ether solvent at 50 °C. The MCs were filtered and washed with DI before testing and exposure to test media. To prevent premature inhibitor release, microcapsules were stored in synthesis solution (pH < 7.2). The microcapsule size and morphology were verified by scanning electron microscope (SEM) using a Tescan Lyra three microscope using 30 kV excitation signal and a working distance of 7 μm. The

microcapsules have been shown to release corrosion inhibitors in solution with pH > 7.2. This occurs due to the deprotonation of colophony (pK_a = 7.2), making the shell increase in solubility, thus increasing the shell porosity, and allowing diffusion of the encapsulated corrosion inhibitor. The release from the microcapsules were studied in-depth in the previous work by the authors (Ress et al., 2020).

The electrochemical tests were carried out in three solutions with varying pH: the near neutral solution of deionized water (pH 6.8) and SCPS (pH 12.6). Both electrolyte solutions were tested with contamination of 0.6 M NaCl, to simulate exposure to marine aggressive environments.

Electrochemical monitoring was performed using a Gamry 600 series potentiostat with a three-electrode setup. The reference electrode used was a saturated calomel electrode (SCE), the counter electrode used was a graphite rod, and the working electrode was a carbon steel rebar. The rebar was prepared by washing and sonicating in ethanol and dried with air. The working area was delimited using non-conductive lacquer to expose the corrugated outer edge of the rebar and connected with a copper wire. First, the open circuit potential (OCP) was conducted for 1 hour, until a steady-state potential was recorded. Secondly, electrochemical impedance spectroscopy (EIS) was performed at OCP using 10 mV r.m.s., a scan range of 10 mHz–100 kHz, and 10 points per decade following ASTM G106-89 (2015). Lastly, potentiodynamic polarization (PDP) scans were conducted from −200 mV_{OCP} to +200 mV_{OCP} and returning to −200 mV_{OCP} with a scan rate of 0.1667 mV/s according to ASTM G61-86 (2018).

The rebars were characterized by scanning electron microscopy (SEM) after exposure using a 30 kV excitation signal and a working distance of 17 µm to image the corrosion products formed. The surface of the rebars exposed to MCs were also analyzed by electron dispersive X-ray spectroscopy (EDX) to study the atomic composition of the surface corrosion products.

Results and discussion

Figure 1 shows an SEM micrograph of colophony microcapsules after filtration. Similar to those shown in the previous study, the microcapsules are spherical in morphology with the presence of pores on the outer shell. The diameter of the microcapsule is variable; however, the average diameter is around 80 µm. The encapsulation efficiency (*EE*) of the microcapsules was calculated by Eq. 1. The determined *EE* was determined to be 85% by induced coupled plasma optical emission spectroscopy.

$$EE = 1 - \frac{[Na^+]_{Supernatant}}{[Na^+]_{Initial}} \quad (1)$$

TABLE 2 Anodic (β_a) and cathodic (β_c) Tafel slopes obtained from polarization tests in DI and SCPS and their corresponding charge transfer coefficients (α_a, α_c) calculated from the Tafel slopes.

	Blank		$NaNO_2$		MC	
Days	**DI**	**SCPS**	**DI**	**SCPS**	**DI**	**SCPS**
			βa (V/decade)			
0	0.033	0.192	0.518	0.133	0.112	0.301
7	0.044	0.130	0.307	0.394	0.178	0.306
14	0.071	0.089	0.457	0.462	0.247	0.549
21	0.068	0.172	0.578	0.551	0.324	0.921
28	0.063	0.151	0.602	0.673	0.387	0.972
			αa			
0	0.910	0.154	0.057	0.222	0.264	0.098
7	0.672	0.227	0.096	0.075	0.166	0.097
14	0.416	0.332	0.065	0.064	0.120	0.054
21	0.435	0.172	0.051	0.054	0.091	0.032
28	0.469	0.196	0.049	0.044	0.076	0.030
			βc (V/decade)			
0	0.059	0.217	0.122	0.131	0.076	0.284
7	0.152	0.158	0.192	0.195	0.083	0.397
14	0.149	0.081	0.182	0.217	0.121	0.319
21	0.136	0.082	0.162	0.254	0.135	0.304
28	0.128	0.088	0.127	0.273	0.156	0.359
			αc			
0	0.501	0.136	0.242	0.226	0.389	0.104
7	0.195	0.187	0.154	0.152	0.356	0.074
14	0.198	0.365	0.162	0.136	0.244	0.093
21	0.217	0.361	0.183	0.116	0.219	0.097
28	0.231	0.336	0.233	0.108	0.190	0.082

Where $[Na^+]_{Supernatant}$ and $[Na^+]_{Initial}$ are the concentrations of Na in the filtered solution after microcapsule synthesis and the initial concentration of Na introduced from $NaNO_2$, respectively.

Figure 2 shows the PDP curves obtained from the steel rebar samples exposed to 0.6 M NaCl in DI solution over the 28 days testing period and the E_{corr} and i_{corr} values obtained are shown in Table 1. The rebar samples in the presence of free $NaNO_2$ inhibitor show the most noble E_{corr} and lowest current density for the majority of the exposure times due to the inhibition mechanism of NO_2^- to form a passive oxide layer composed of maghemite (Fe_2O_3) and lepidocrocite (γ-FeOOH) (Dhouibi et al., 2003). The most noble samples, Day 0, measured the most noble E_{corr} value of −144 mV_{SCE} as the initial passive layer developed by the corrosion inhibitors has not been depleted from chloride exposure. However, as exposure time increases, the i_{corr} increases up to 4.24 ×10^{-6} A/cm^2, denoting a loss of corrosion inhibition effectiveness while maintaining values that are lower than the

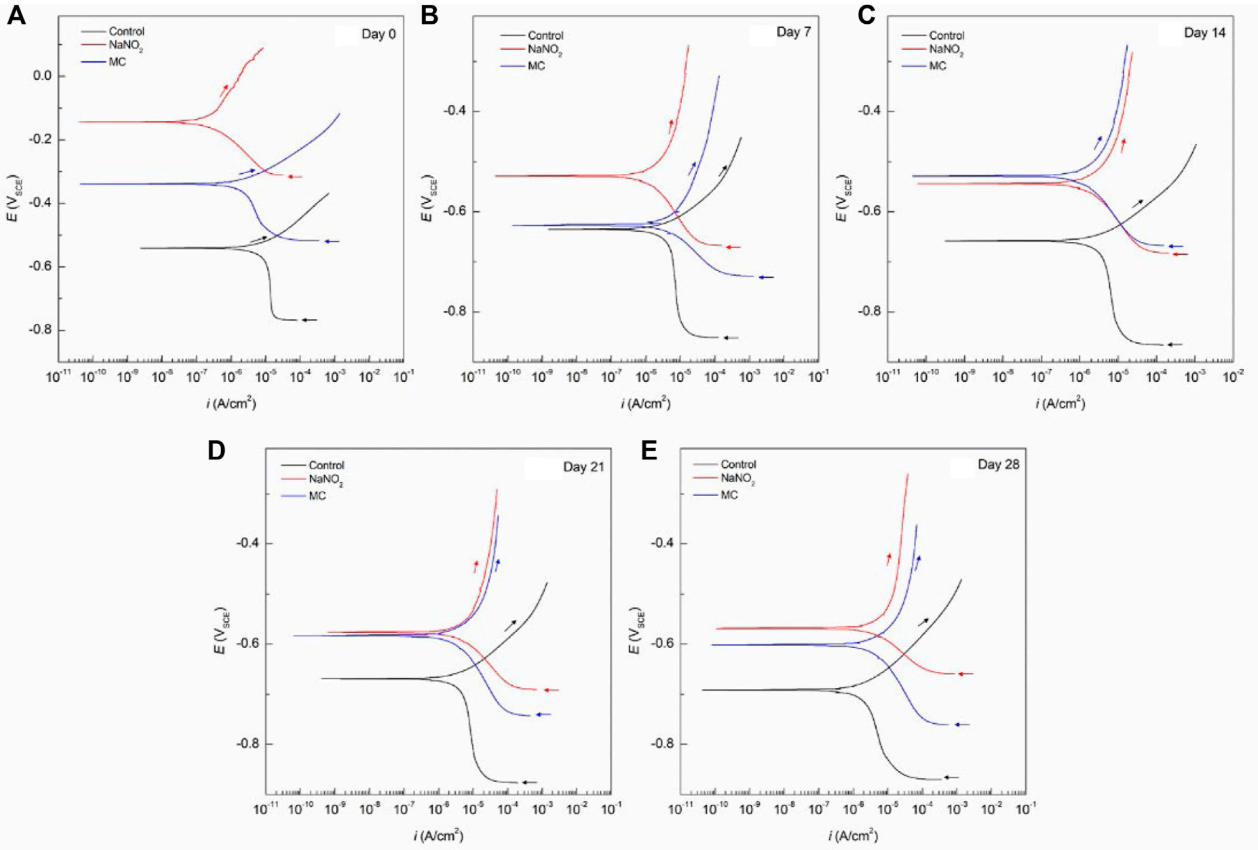

FIGURE 3
Potentiodynamic polarization curves obtained for carbon steel rebars immersed in SCPS with 0.6 M NaCl for the control sample, free $NaNO_2$ corrosion inhibitor sample, and colophony MCs samples after different time exposure: **(A)** 0 days, **(B)** 7 days, **(C)** 14 days, **(D)** 21 days, and **(E)** 28 days.

control. The loss of corrosion inhibition of nitrites has been shown with exposure to chlorides, as the aggressive agents are able to cause passivity breakdown of the surface. The MC samples initially display values of E_{corr} and i_{corr} between the free inhibitor and blank samples. After 7 days of exposure, however, the MC exposed samples show both E_{corr} and i_{corr} values similar to the free inhibitor samples due to the release mechanism of the MC. The anodic kinetic parameters, shown in Table 2, highlight the inhibitor mechanism, as the anodic Tafel slope (β_a) increases in the presence of $NaNO_2$ compared to the control. The free inhibitor samples show βa of 0.518 V/dec, higher than the control with 0.033 V/dec, thus showing reduced anodic dissolution. Initially, the MC exposed rebar at day 0 shows low inhibition due to the low pH of 6.8 of the DI-water solution, below the pK_a of colophony (7.2), corresponding to a slow inhibitor release (Ress et al., 2020). As exposure time increases, β_a increases to 0.387 V/dec and the β_c increases to 0.156 V/dec. From the i_{corr} values, it can be seen that both the free $NaNO_2$ inhibitor and the MC samples are above the threshold for active corrosion (1 μA/cm^2), yet they are close in value and nearly half the i_{corr} value of the control sample (9.21 ×10^{-6} A/cm^2).

Figure 3 shows the PDP curves for the carbon steel rebars exposed to 0.6 M NaCl in SCPS. The free inhibitor samples show more noble E_{corr} values (−548 mV_{SCE}) and current densities near 1 μA/cm^2 after the 28 days exposure time. The free inhibitor sample showed a similar E_{corr} of −613 mV_{SCE} with a higher i_{corr} than the MC sample with 4.26 ×10^{-6} A/cm^2, nearly twice the MC value. By analyzing the i_{corr} values for the SCPS exposed samples, all samples initially show a lower risk of corrosion for the initial test, however, the samples exposed to the chlorinated solution for 7 days and longer show values above the 1 μA/cm^2 threshold. The MCs exposed samples show the most significant effect on β_c, showing a final value of 0.359 V/dec, thus the largest contribution from the colophony on the corrosion inhibition (Brocas et al., 2014). The MC samples also show higher potentials than the control in all the tested

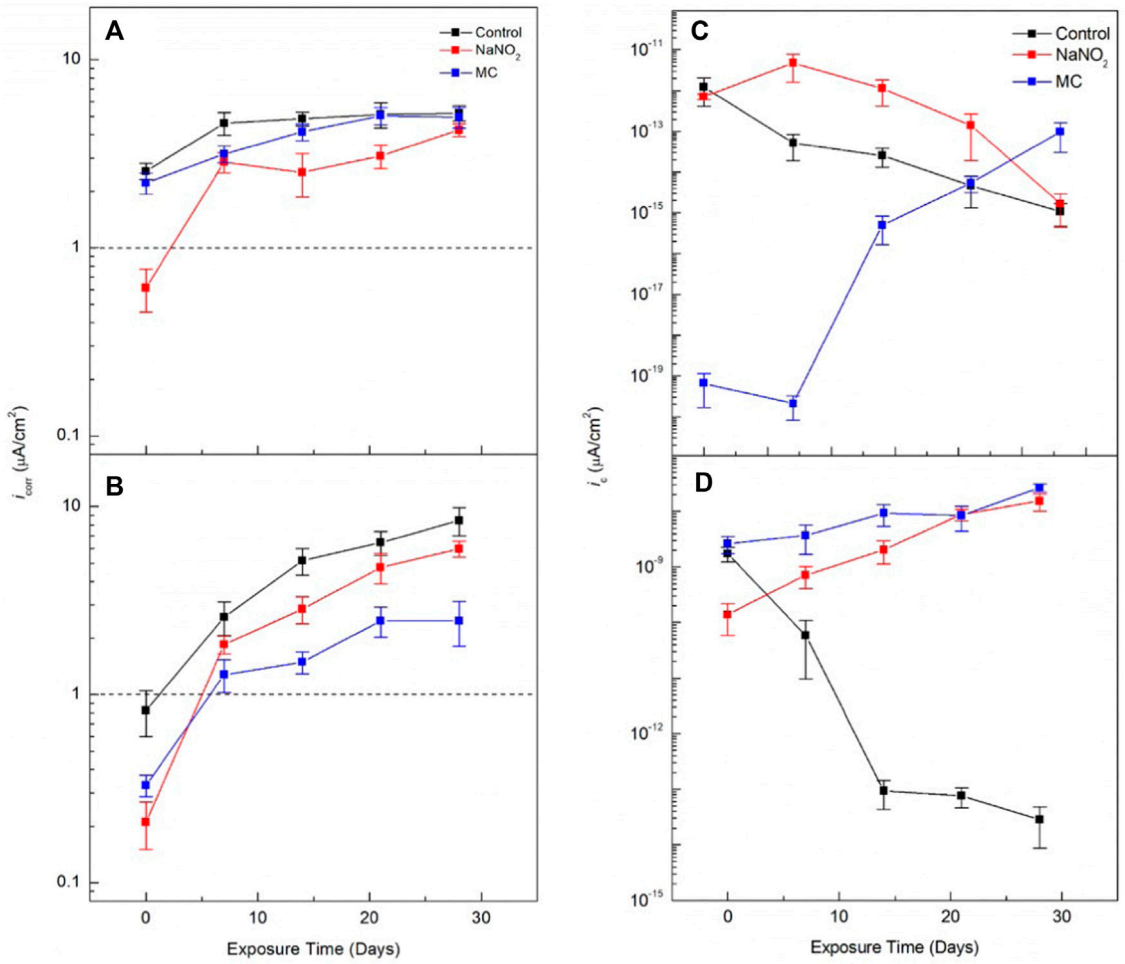

FIGURE 4
Corrosion current density (i_{corr}) of carbon steel rebars in the presence of $NaNO_2$ corrosion inhibitors and colophony microcapsules containing $NaNO_2$ in **(A)** DI water (pH 6.8) and **(B)** SCPS (pH 12.6), contaminated with 0.6 M NaCl, and cathodic exchange current densities (i_c) measurements in **(C)** DI and **(B)** SCPS.

TABLE 3 Cathodic exchange current density (i_c) values for the exposed rebar samples.

Days	Control		$NaNO_2$		MC	
	DI	SCPS	DI	SCPS	DI	SCPS
			i_c (A/cm^2)			
0	1.24×10^{-12}	1.74×10^{-9}	7.11×10^{-13}	1.39×10^{-10}	6.63×10^{-20}	2.64×10^{-9}
7	5.11×10^{-14}	5.89×10^{-11}	4.72×10^{-12}	7.13×10^{-10}	2.05×10^{-20}	3.68×10^{-9}
14	2.55×10^{-14}	9.36×10^{-14}	1.14×10^{-12}	2.03×10^{-9}	4.92×10^{-16}	9.29×10^{-9}
21	4.58×10^{-15}	7.61×10^{-14}	1.40×10^{-13}	8.76×10^{-9}	5.44×10^{-15}	8.35×10^{-9}
28	1.07×10^{-15}	2.87×10^{-14}	1.68×10^{-15}	1.52×10^{-8}	9.69×10^{-14}	2.66×10^{-8}

TABLE 4 Anodic (β_a) and cathodic (β_c) Tafel slopes obtained from polarization tests in DI and SCPS and their corresponding charge transfer coefficients (α_a, α_c) calculated from the Tafel slopes.

	Blank		$NaNO_2$		MC	
Days	**DI**	**SCPS**	**DI**	**SCPS**	**DI**	**SCPS**
			βa (V/decade)			
0	0.033	0.192	0.518	0.133	0.112	0.301
7	0.044	0.130	0.307	0.394	0.178	0.306
14	0.071	0.089	0.457	0.462	0.247	0.549
21	0.068	0.172	0.578	0.551	0.324	0.921
28	0.063	0.151	0.602	0.673	0.387	0.972
			αa			
0	0.910	0.154	0.057	0.222	0.264	0.098
7	0.672	0.227	0.096	0.075	0.166	0.097
14	0.416	0.332	0.065	0.064	0.120	0.054
21	0.435	0.172	0.051	0.054	0.091	0.032
28	0.469	0.196	0.049	0.044	0.076	0.030
			βc (V/decade)			
0	0.059	0.217	0.122	0.131	0.076	0.284
7	0.152	0.158	0.192	0.195	0.083	0.397
14	0.149	0.081	0.182	0.217	0.121	0.319
21	0.136	0.082	0.162	0.254	0.135	0.304
28	0.128	0.088	0.127	0.273	0.156	0.359
			αc			
0	0.501	0.136	0.242	0.226	0.389	0.104
7	0.195	0.187	0.154	0.152	0.356	0.074
14	0.198	0.365	0.162	0.136	0.244	0.093
21	0.217	0.361	0.183	0.116	0.219	0.097
28	0.231	0.336	0.233	0.108	0.190	0.082

solutions due to the passive film formation in alkaline media as well as the larger burst release from the microcapsules. Additionally, the MCs exposed samples show the most significant effect on β_c, showing a final value of 0.359 V/dec, thus the largest contribution from the colophony on the corrosion inhibition, as nitrite acts only as an anodic inhibitor. The authors previously showed the oxidation of the colophony shell after exposure to aqueous solution, thus the oxidation of abietic acid consumes available dissolved oxygen, reducing the cathodic reaction kinetics and acting as an oxygen scavenger. Furthermore, the π-electrons of the abietic acid suggests it acts as an effective organic corrosion inhibitor for steel (Mohamed et al., 2021). Therefore, the improved corrosion protection afforded by the MCs can be attributed to a multi-inhibition system of the released $NaNO_2$ corrosion inhibitors facilitating passive film formation and oxygen scavenging by the colophony shell. The anodic kinetics also show significant increase to a β_a value of 0.972 mV/dec. This is caused by the pH triggered release, which is highest in the alkaline SCPS solution (Ress et al., 2020).

The i_{corr} values obtained from the curves through Tafel analysis were plotted in Figures 4A,B and the inhibition efficiency (IE) were calculated using Eq. 2 to analyze the polarization data and observe its trends over time more clearly, see Table 1.

$$IE(\%) = \frac{i_{corr,control} - i_{corr,inhibitor}}{i_{corr,control}} \times 100 \quad (2)$$

Where $i_{corr,\ control}$ is the corrosion current density of the control sample with no inhibitor and $i_{corr,\ inhibitor}$ is the corrosion current density of the free inhibitor or MC sample. The MC samples show a significant decrease of the IE compared to the free inhibitor, 73% and 93%, respectively. However, after 7 days of exposure, the values were similar, ending with 47% and 42% for the free $NaNO_2$ and MC samples, respectively. For SCPS, all samples initially show a lower IE. For the 28 days of exposure, the release from the microcapsules was sufficient to cause improved IE values compared to the free $NaNO_2$ sample.

The change in the cathodic kinetics observed in the polarization curves was further analyzed by calculating the cathodic exchange current density (i_c), which describes the kinetics of the oxygen reduction reaction (ORR) shown in Eq. 3:

$$O_{2\,(g)} + 2H_2O + 4e^- \rightarrow 4OH^- \quad (3)$$

The Butler-Volmer equation in Eq. 4 can be utilized to calculate i_c, see Table 3:

$$i_c = i_{corr} \exp\left[-\frac{\alpha_c n F \eta_c}{RT}\right] \quad (4)$$

Where n is the number of electrons involved in the cathodic reaction, F is the Faraday constant, η_c is the activation overpotential ($\eta_c = E_{ORR} - E_{corr}$), α_c is the charge transfer coefficient of cathodic reaction, R and T are the ideal gas constant and temperature, respectively. The E_{ORR} values were obtained from literature to be +162 mV_{SCE}, and +581 mV_{SCE} for DI (pH 6.8) and SCPS (pH 12.6), respectively (Beverskog and Puigdomenech, 1996). The E_{ORR} is the electrochemical potential at which oxygen will be reduced in solution to hydroxide ions. Figures 4C,D shows the calculated i_c values for the control, free $NaNO_2$, and MC samples. The free $NaNO_2$ samples display an initial decrease in ic from 7.11 $\times 10^{-13}$ A/cm^2 to 1.68 $\times 10^{-15}$ A/cm^2 after 28 days of exposure, indicating the lack of cathodic inhibition, as the cathodic kinetics is similar to the control, thus the corrosion inhibition is strictly imparted from the anodic corrosion inhibitors. The MC samples, however, show lower values. This is caused by the addition of the colophony microcapsules and the oxidation effect of colophony, see Figure 1B (Ren et al., 2015). Tannins and other organic

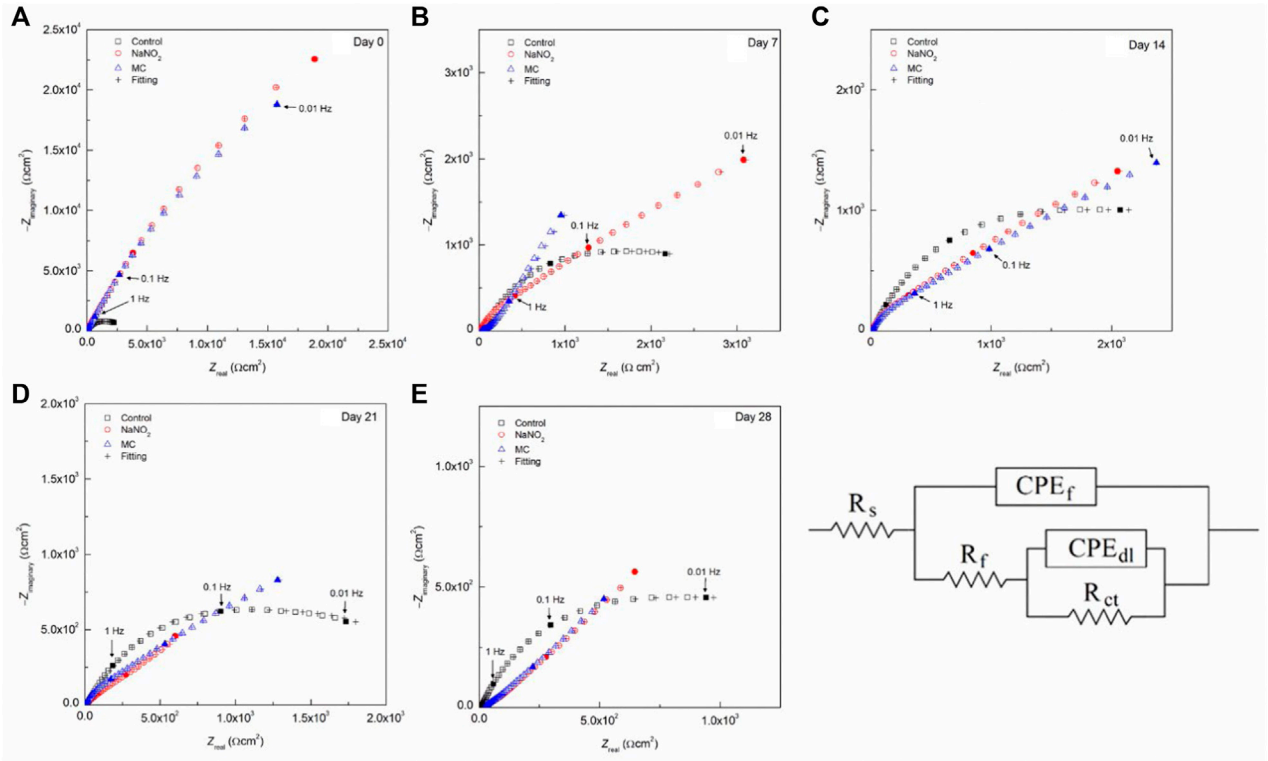

FIGURE 5
Nyquist plots for carbon steel rebars in the presence of $NaNO_2$ corrosion inhibitors and colophony microcapsules containing $NaNO_2$ in DI water (pH 6.8) contaminated with 0.6 M NaCl after different time exposure: **(A)** 0 days, **(B)** 7 days, **(C)** 14 days, **(D)** 21 days, and **(E)** 28 days. The equivalent circuit used for fitting the EIS is also shown.

TABLE 5 EIS fitting parameters obtained for carbon steel rebar in DI water contaminated with 0.6 M NaCl.

Days		R_s Ω cm^2	R_f Ω cm^2	R_{ct} Ω cm^2	Y_f S/cm^2 s^{n,f}	n_f	Y_{dl} S/cm^2 s^{n,dl}	n_{dl}	χ^2 (*)	$C_{eff,dl}$ F/cm^2
0	Control	10	45	2.8×10^3	2.90×10^4	0.63	2.15×10^4	0.74	7.70×10^{-4}	2.53×10^{-5}
	$NaNO_2$	9	358	8.3×10^4	1.82×10^4	0.73	5.26×10^5	0.76	5.88×10^{-4}	4.66×10^{-6}
	MC	12	28	5.0×10^3	3.90×10^4	0.71	1.30×10^4	0.79	2.56×10^{-4}	2.20×10^{-5}
7	Control	18	50	2.9×10^3	1.83×10^4	0.71	1.20×10^3	0.74	2.01×10^{-4}	5.33×10^{-5}
	$NaNO_2$	14	516	9.3×10^3	3.60×10^4	0.73	9.86×10^4	0.78	3.70×10^{-4}	2.22×10^{-5}
	MC	11	25	1.9×10^4	3.90×10^4	0.68	1.37×10^4	0.64	8.65×10^{-4}	3.75×10^{-6}
14	Control	18	39	3.1×10^3	5.93×10^4	0.78	9.51×10^4	0.72	1.41×10^{-4}	3.65×10^{-4}
	$NaNO_2$	16	452	2.3×10^3	5.60×10^4	0.72	8.51×10^4	0.69	1.21×10^{-4}	1.23×10^{-4}
	MC	13	36	8.1×10^3	6.50×10^4	0.69	2.34×10^4	0.78	2.54×10^{-4}	4.56×10^{-5}
21	Control	17	24	2.4×10^3	1.80×10^3	0.62	1.96×10^3	0.72	4.30×10^{-4}	5.21×10^{-4}
	$NaNO_2$	10	165	1.1×10^3	2.04×10^3	0.72	3.23×10^3	0.79	7.31×10^{-5}	1.30×10^{-4}
	MC	14	51	1.0×10^4	8.90×10^4	0.81	3.69×10^4	0.71	3.21×10^{-4}	4.29×10^{-5}
28	Control	11	22	2.2×10^3	3.40×10^3	0.74	2.39×10^3	0.73	6.27×10^{-4}	6.21×10^{-4}
	$NaNO_2$	11	120	1.0×10^3	2.41×10^3	0.76	2.57×10^3	0.76	3.68×10^{-4}	1.51×10^{-4}
	MC	20	65	2.4×10^4	1.80×10^3	0.61	1.47×10^3	0.69	3.49×10^{-5}	1.09×10^{-4}

(*) Total error <10%.

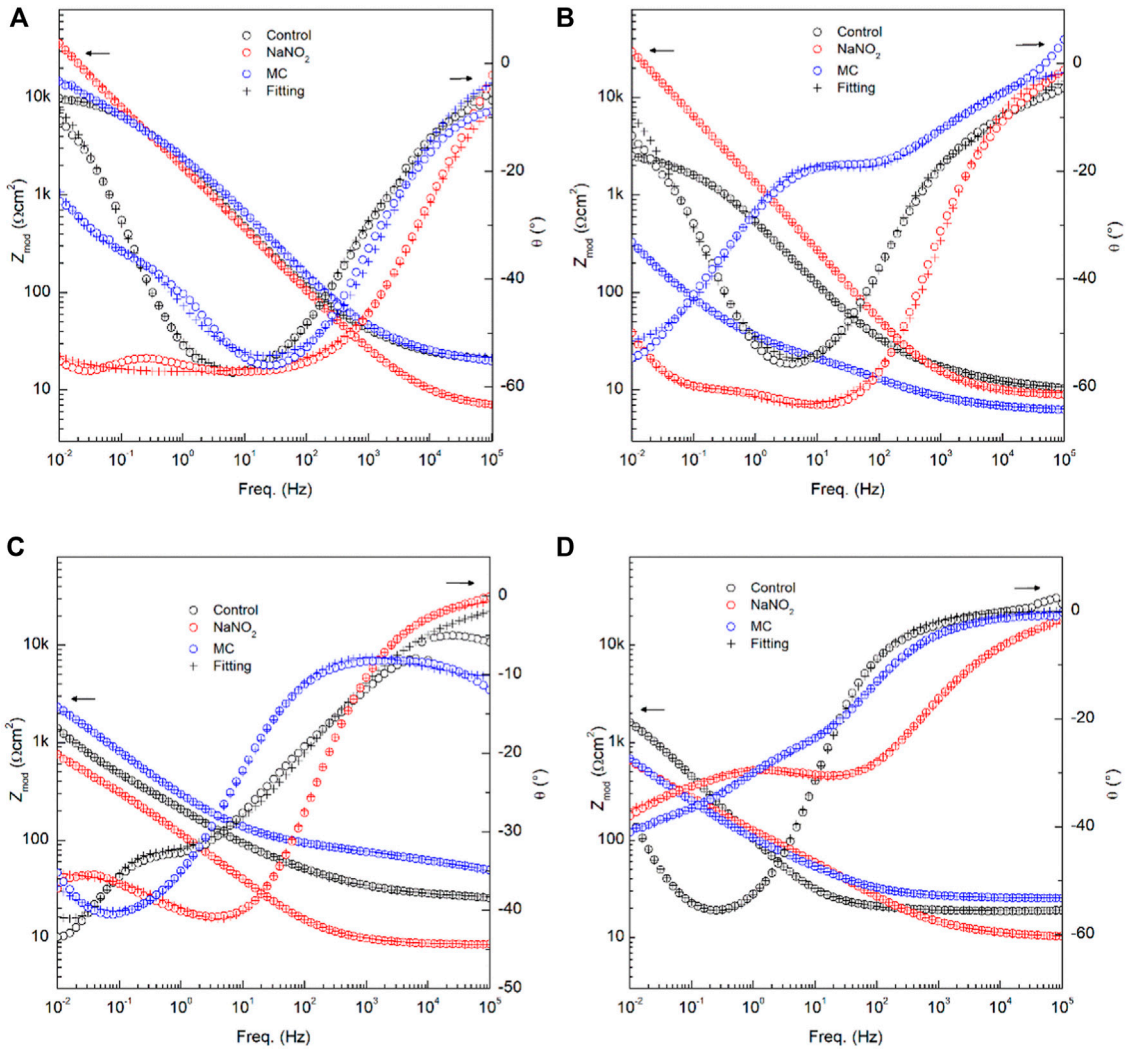

FIGURE 6
Bode plots showing experimental and fitting data obtained from EIS analysis for carbon steel rebars in the presence of $NaNO_2$ corrosion inhibitors and colophony microcapsules containing $NaNO_2$: **(A)** 0 days in DI water, **(B)** 0 days in SCPS, **(C)** 28 days in DI water, and **(D)** 28 days in SCPS.

molecules have been shown to exhibit oxygen scavenging activity and have been used as such in the food processing industry and pharmaceutical industries (Dave and Shah, 1997). Lastly, the MC samples show the largest difference of i_c in this solution, with values of 2.64 $\times 10^{-9}$ A/cm^2, over two orders of magnitude lower than the control after 28 days of exposure.

The charge transfer coefficient, α, is a parameter depicting the symmetry of the energy barrier for the electrochemical corrosion reaction (anodic α_a and cathodic α_c) (Antonello and Maran, 1999). The transfer coefficient can be calculated from the relationship in Eq. (5) (Bauer, 1968):

$$\alpha = \frac{2.303RT}{\beta nF} \tag{5}$$

where β is the Tafel coefficient obtained from the potentiodynamic polarization data. The α values are shown in Table 4. The changes in α, while highlighting the reaction symmetry of the energy barrier, is dependent upon both potential and surface coverage for organic species (Kornyshev and Schmickler, 1986). Additionally, the solvation of organic molecules can account for small changes in α, denoting outer-sphere reorganization (Savéant and Tessier, 1982). In the colophony microcapsule, dissolution of the shell, as well as changes in the charge transfer resistance and increased surface coverage of the rebar sample, lead to decreasing values in α_c, reaching values below 0.1, showing a non-reversible electron transfer

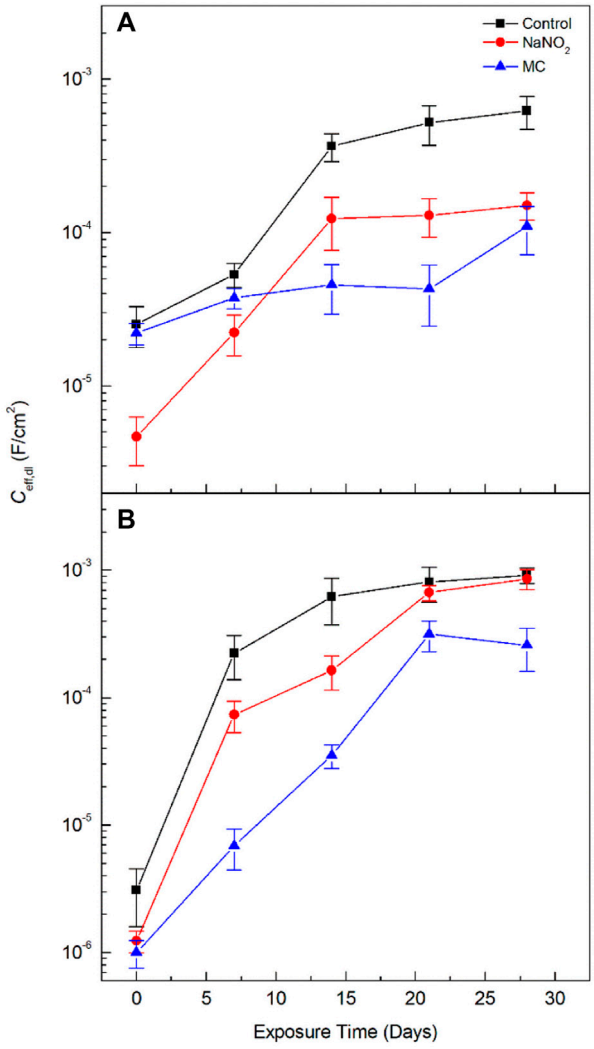

FIGURE 7
The calculated $C_{eff,dl}$ values for **(A)** DI, and **(B)** SCPS contaminated with 0.6 M NaCl.

(α = 0.5 for reversible reactions) (Bauer, 1968). This decrease in cathodic activity evidence the influence of colophony oxidation consuming dissolved oxygen and reducing the cathodic reaction of the rebar, thus acting as an oxygen scavenger. These values deviating from 0.5 highlight the asymmetric polarization of the rebar, while the control and free $NaNO_2$ inhibitor exposed samples have higher values close to 0.5. This variance is attributed to the cathodic inhibition and oxygen scavenging nature of the colophony shell, whose adsorption onto the rebar and depletion of dissolved oxygen influence the cathodic kinetics for exposed samples.

The EIS results obtained in DI with 0.6 M NaCl shown in Figure 5 and Table 5 indicate poor inhibition of the MCs in DI water relative to free inhibitors, due to low release. In the obtained experimental spectra, two regions can be clearly distinguished: a high frequency region, where the ohmic drop is controlled by the electrolyte solution resistance, and a low-frequency region, in which the relaxation process is governed by the electrochemical behavior of the metal-electrolyte interface. The Nyquist spectra obtained during the initial period reveals that the experimental data obtained can be adequately fitted using the electrical equivalent circuit (EEC) shown in Figure 5. In this EEC, Rs represents the electrolyte solution resistance. The R_f is the resistance offered by the passive layer, and the constant phase element (CPE_f) corresponds to the pseudocapacitive behavior of this passive oxide film. The anodic dissolution process induced by Cl^-localized corrosion attack is represented using R_{ct} for the charge transfer resistance inside the pits, and CPE_{dl} for pseudocapacitive behavior of the double layer. Each *CPE* accounts for the non-ideal capacitance response and depends on the capacitance and on a dimensionless parameter (n) that represents the nonideality of the *CPE*. The Nyquist plots show an increasing trend for both R_f and R_{ct} values for MC specimens, reaching 65 Ω cm^2 and 2.4 $\times 10^4$ Ω cm^2 for R_f and R_{ct}, respectively, thus promoting passive film formation, showing the best corrosion resistance after 28 days of release and exposure. The R_f of the MCs show values near 50 Ω cm^2, less than free inhibitor which shows decreasing values over time as the chloride is able to depassivate the rebar. Similarly, the R_{ct} values show the same trend until the final measurement, demonstrating a higher corrosion resistance than the free inhibitor. The Bode plots are shown in Figure 6 for 0 days and 28 days of exposure in solution including the fitting results with the proposed EEC. It can be seen that the plots show a good fitting with the proposed EEC and display a two-time constant behaviour even after prolonged exposure to the test solutions. The phase angle (θ) shows two inflection points, thus indicating two relaxion processes, i.e., two time constants. Additionally, the impedance modulus (Z_{mod}) corroborates the polarization results, showing the improved performance of the MC samples after 28 days of exposure due to higher Z_{mod} values in SCPS. Furthermore, the similarity in the Z_{mod} between the free $NaNO_2$ and MC samples are consistent with polarization results.

Additionally, the effective capacitance for the electrochemical double layer can be determined according to Eq. 6 (Brug et al., 1984):

$$C_{eff,dl} = Y_{dl}^{1/n_{dl}} \left(\frac{1}{R_s} + \frac{1}{R_{ct}} \right)^{(n_{dl}-1)/n_{dl}} \quad (6)$$

where $C_{eff,dl}$ is the effective double layer capacitance; Y_{dl} is the admittance; n_{dl} is the *CPE* exponents of the electrochemical double layer, R_s is the solution resistance, and R_{ct} is the charge transfer resistance. $C_{eff,dl}$ was calculated

TABLE 6 EIS fitting parameters obtained for carbon steel rebar in SCPS contaminated with 0.6 M NaCl.

Days		R_s Ω cm^2	R_f Ω cm^2	R_{ct} Ω cm^2	Y_f S/cm^2 s^{n,f}	n_f	Y_{dl} S/cm^2 s^{n,dl}	n_{dl}	χ^2 (*)	$C_{eff,dl}$ F/cm^2
0	Control	20	47	1.1×10^4	6.12×10^{-4}	0.69	5.84×10^{-5}	0.70	3.13×10^{-4}	3.08×10^{-6}
	$NaNO_2$	12	588	5.4×10^5	1.62×10^{-4}	0.63	2.41×10^{-6}	0.94	1.17×10^{-3}	1.24×10^{-6}
	MC	13	527	6.3×10^4	4.77×10^{-4}	0.75	1.06×10^{-5}	0.79	4.04×10^{-4}	9.98×10^{-7}
7	Control	10	857	4.2×10^3	2.52×10^{-4}	0.65	1.57×10^{-3}	0.68	5.20×10^{-4}	2.23×10^{-4}
	$NaNO_2$	9	3,611	7.1×10^3	2.12×10^{-4}	0.66	6.62×10^{-4}	0.70	1.90×10^{-3}	7.36×10^{-5}
	MC	17	602	1.5×10^4	4.82×10^{-4}	0.68	4.59×10^{-4}	0.74	1.68×10^{-4}	6.87×10^{-6}
14	Control	11	573	5.0×10^3	6.85×10^{-4}	0.81	2.14×10^{-3}	0.71	9.60×10^{-4}	6.19×10^{-4}
	$NaNO_2$	15	1856	6.9×10^3	3.40×10^{-5}	0.74	1.19×10^{-3}	0.67	1.05×10^{-3}	1.64×10^{-4}
	MC	29	1,272	8.0×10^3	5.04×10^{-5}	0.72	1.49×10^{-3}	0.78	1.47×10^{-4}	3.51×10^{-5}
21	Control	25	1,621	3.8×10^3	2.28×10^{-3}	0.72	1.01×10^{-3}	0.68	7.16×10^{-4}	8.09×10^{-4}
	$NaNO_2$	17	2,431	5.2×10^3	1.08×10^{-4}	0.69	1.87×10^{-3}	0.77	4.92×10^{-4}	6.67×10^{-4}
	MC	21	3,649	7.1×10^3	8.60×10^{-5}	0.85	2.46×10^{-3}	0.74	2.31×10^{-4}	3.14×10^{-4}
28	Control	23	951	1.6×10^3	2.87×10^{-3}	0.76	1.12×10^{-3}	0.83	5.02×10^{-3}	9.11×10^{-4}
	$NaNO_2$	19	1,587	5.9×10^3	1.28×10^{-4}	0.86	2.04×10^{-3}	0.79	1.86×10^{-4}	8.59×10^{-4}
	MC	20	2,684	7.9×10^3	1.03×10^{-4}	0.80	3.67×10^{-3}	0.85	6.04×10^{-4}	2.31×10^{-4}

(*) Total error <10%.

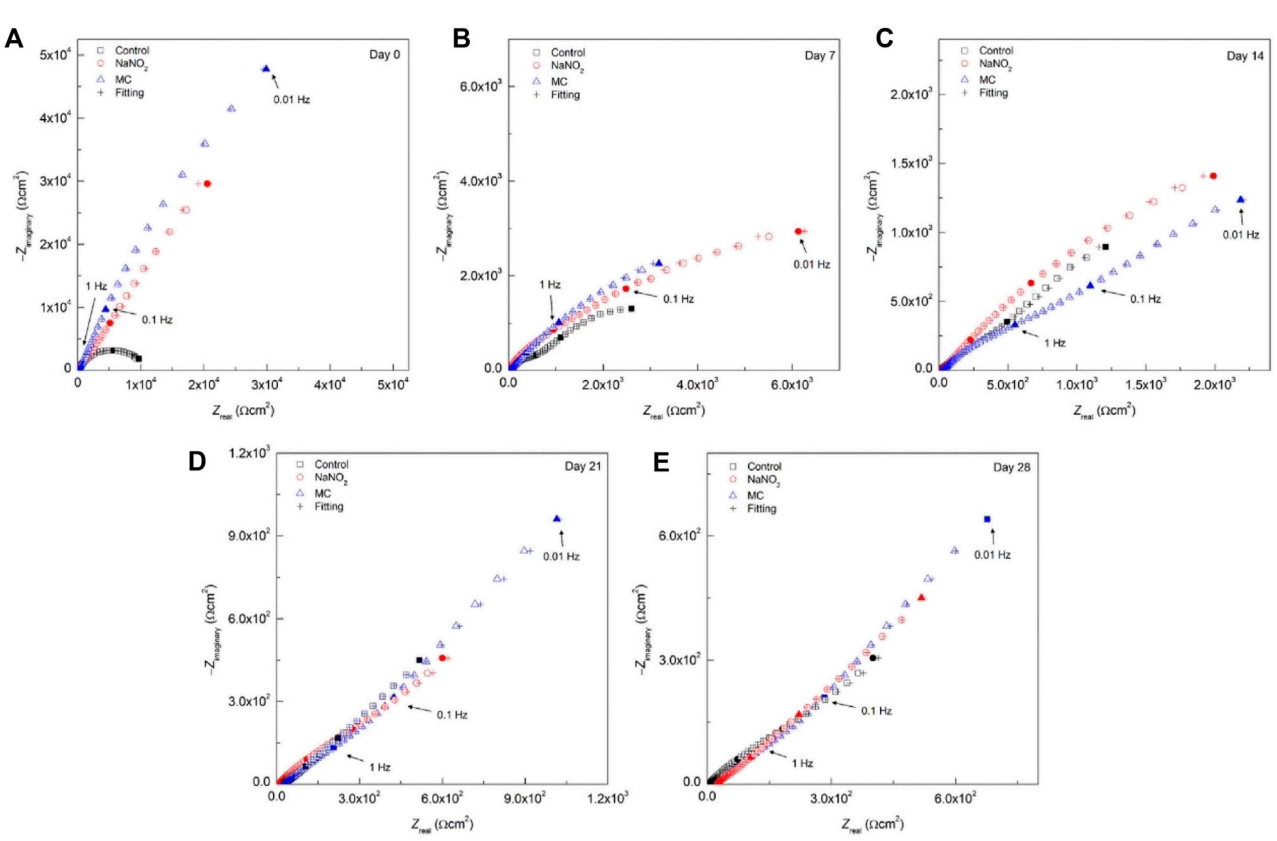

FIGURE 8
Nyquist plots for carbon steel rebars in the presence of $NaNO_2$ corrosion inhibitors and colophony microcapsules containing $NaNO_2$ in SCPS (pH 12.6) contaminated with 0.6 M NaCl after different time exposure: **(A)** 0 days, **(B)** 7 days, **(C)** 14 days, **(D)** 21 days, and **(E)** 28 days.

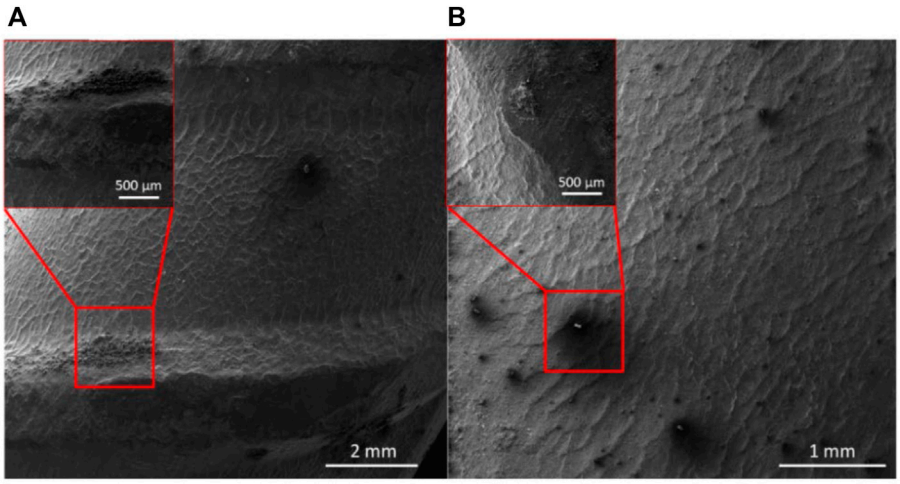

FIGURE 9
SEM images of carbon steel rebars exposed to SCPS with **(A)** 0.6 M NaCl and MCs, and **(B)** 0.6 M NaCl and $NaNO_2$ corrosion inhibitors.

(see Figure 7 and Table 5 and Table 6 for DI water and SCPS, respectively).

The EIS results for SCPS are shown in Figure 8 and Table 6. Both the R_f and R_{ct} of the MC exposed specimens show enhanced values compared to the free $NaNO_2$, 2.7 $\times 10^3\ \Omega\ cm^2$ and 7.9 $\times 10^3\ \Omega\ cm^2$, respectively. These results validate the DC testing, indicating enhanced corrosion protection imparted by the MCs, as the MC exposed samples impedance is greater than the free inhibitor alone. Unlike the results obtained for DI, the protection of the MCs in the alkaline SCPS are exhibited immediately, as the alkaline release is triggered, the inhibitors are released. The R_f value for the MC specimens helps substantiate the development of the protective oxide passive film. The free inhibitor sample shows an initial increase from 588 $\Omega\ cm^2$ to 3,611 $\Omega\ cm^2$, showing a quick development, however, the MC sample surpasses the free inhibitor, a result from triggered release and shows a higher R_f for the remaining test periods. The $C_{eff,dl}$ values are shown in Figure 7. In DI water, the $C_{eff,dl}$ values obtained for the 28 days exposed samples in the presence of free $NaNO_2$ corrosion inhibitor displayed a $C_{eff,dl}$ value of 1.51 $\times 10^{-4}\ F\ cm^{-2}$, close to the MC sample with 1.09 $\times 10^{-4}\ F\ cm^{-2}$, thus indicating similar anticorrosion performance. The MC exposed specimens in SCPS show the greatest difference with $C_{eff,dl}$ values an order of magnitude lower than the free inhibitor for the first 14 days of exposure. Subsequently, the MC exposed specimens show lower capacitance than the inhibitor ending the test duration with a $C_{eff,dl}$ value of 2.31 $\times 10^{-4}\ F\ cm^{-2}$ compared to the free inhibitor with 8.59 $\times 10^{-4}\ F\ cm^{-2}$, almost four times lower. More importantly the $C_{eff,dl}$ shows for the MC shows almost one order of magnitude lower than the free inhibitors for all time periods, thus a lower susceptibility to corrosion. These results corroborate the improved corrosion inhibition efficiency for the MC in alkaline pH as further deprotonation of the colophony occurs and undergoes oxidation, thus more inhibitor molecules are released.

The SEM images in Figure 9 shows the free inhibitor and MC rebars exposed to SCPS contaminated with 0.6 M NaCl after 28 days of exposure. The MC specimens have visibly less corrosion products on the rebar surface compared to the free inhibitor. The corrosion products are most heavily concentrated on the rebar corrugations, where the geometry of the rebar and residual stresses created during manufacturing promote anodic dissolution (Bautista et al., 2019). Both rebar specimens show corrosion products near the corrugated section and some locations between the corrugations. Additionally, the MC exposed rebar showed microcapsules adhered to the surface of the rebar.

In the images shown by Figures 10A,B MCs can be seen adsorbed to the rebar surface. This adsorption suggests that colophony shell of the MCs is indeed playing a more significant role in the inhibition process. Recently, researchers synthesized an imidazoline corrosion inhibitor using colophony, concluding that the new rosin-based inhibitors adsorbed to the metal surface and increased inhibition of imidazoline (Geng et al., 2022). EDX analysis was performed on the rebar exposed to MC in SCPS on locations 1) and (2). The elemental composition shows a large concentration of O, Fe, and Cl atoms. This underlines

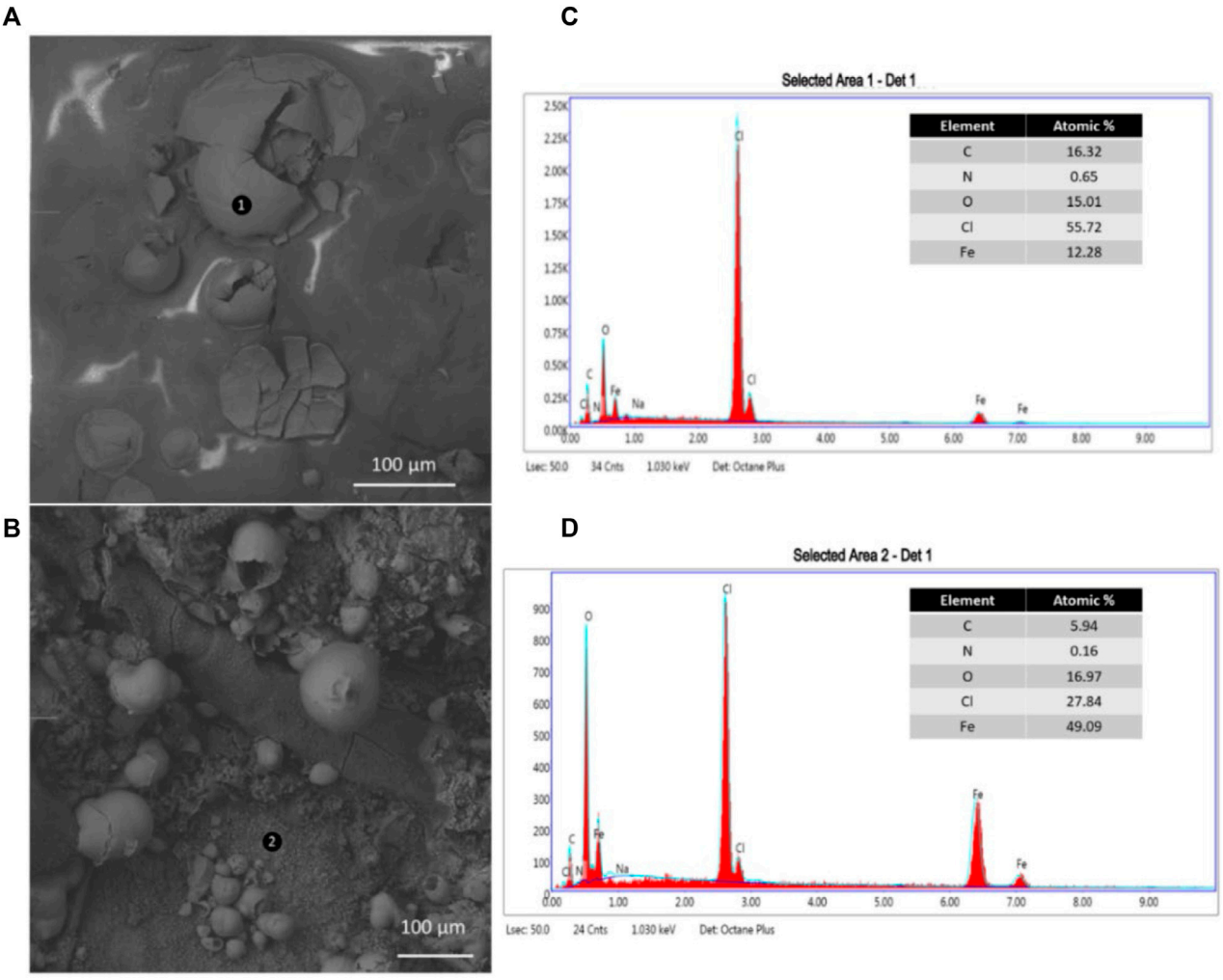

FIGURE 10
SEM images, **(A)** and **(B)**, of and MCs adsorbed to the rebar surface after 28 days exposure to SCPS contaminated with 0.6 M NaCl. The EDX spectra obtained from **(C)**, point (1), and **(D)**, point (2), from the SEM images for the MC surface elemental composition and the composition of the rust, respectively.

the large amount of oxidation of the MCs as well as chloride adsorption onto the MC shell. Smaller amounts of Na and N are seen from the $NaNO_2$ inhibitors encapsulated in the MCs. The SEM and EDX results corroborate the electrochemical tests, showing the ability of the MCs containing corrosion inhibitor to protect carbon steel.

Conclusions

Colophony microcapsules containing $NaNO_2$ corrosion inhibitor were synthesized by W/O/W double emulsion method. The corrosion protection of the microcapsules was studied over 28 days in varying pH solutions containing chlorides. The following conclusions can be made:

- The colophony MCs releasing $NaNO_2$ corrosion inhibitor showed improved corrosion resistance in DI and SCPS solutions contaminated with 0.6 M NaCl. The MC exposed samples displayed improved i_{corr} values (2.54×10^{-6} A/cm^2) compared to free $NaNO_2$ inhibitors (5.96×10^{-6} A/cm^2).
- The cathodic Tafel slopes of the MC exposed samples show decreased cathodic kinetics from the addition of the colophony shell, as the abietic acid oxidizes and absorbs to the rebar surface, providing cathodic inhibition in addition to the release of nitrite inhibitors reducing the anodic kinetics. The change in cathodic kinetics is, in part, due to the oxygen scavenging of the abietic acid, oxidizing the abietic acid similar to mechanisms shown in literature for hydroquinone and henna extract.

- The analysis of the EIS data showed increased charge transfer resistance for the MC exposed samples in SCPS. Additionally, calculations of the $C_{eff,dl}$ showed the MC exposed samples having improved corrosion resistance compared to the free $NaNO_2$ samples, especially after 28 days of exposure. (Gaikwad et al., 2020), (Keserovic and Birketveit, 2021), (Sastri and Malaiyandi, 1983), (Yan et al., 2013)

Data availability statement

The datasets presented in this article are not readily available because The raw/processed data required to reproduce these findings cannot be shared at this time as the data also forms part of an ongoing study. Requests to access the datasets should be directed to dbastidas@uakron.edu.

Author contributions

Conceptualization, DMB; methodology, JR, and DMB; formal analysis, JR, UM and DMB; investigation, JR, UM and DMB; resources, DMB; data curation, JR and DMB; writing—original draft preparation, JR, and DMB; writing—review and editing, JR and DMB; visualization, DMB; supervision, DMB; project administration, DMB; funding acquisition, DMB. All authors have read and agreed to the published version of the manuscript.

Funding

This research was funded by Firestone Research, grant number 639430, and The University of Akron Fellowship, grant numbers FRC-207160 and FRC-207865.

Acknowledgments

The authors acknowledge the technical support and facilities from The National Center for Education and Research on Corrosion and Materials Performance (NCERCAMP-UA), The College of Engineering and Polymer Science and The University of Akron.

Conflict of interest

The authors declare that the research was conducted in the absence of any commercial or financial relationships that could be construed as a potential conflict of interest.

Publisher's note

All claims expressed in this article are solely those of the authors and do not necessarily represent those of their affiliated organizations, or those of the publisher, the editors and the reviewers. Any product that may be evaluated in this article, or claim that may be made by its manufacturer, is not guaranteed or endorsed by the publisher.

References

Al-Ameeri, A. S., Rafiq, M. I., and Tsioulou, O. (2021). Combined impact of carbonation and crack width on the chloride penetration and corrosion resistance of concrete structures. *Cem. Concr. Compos* 115, 103819. doi:10.1016/j.cemconcomp.2020.103819

Andrade, C. (2020). Evaluation of the degree of carbonation of concretes in three environments. *Constr. Build. Mater* 230, 116804. doi:10.1016/j.conbuildmat.2019.116804

Antonello, S., and Maran, F. (1999). The role and relevance of the transfer coefficient α in the study of dissociative electron transfers: Concepts and examples from the electroreduction of perbenzoates. *J. Am. Chem. Soc.* 121, 9668–9676. doi:10.1021/ja991407a

ASTM G106-89 (2015). *Standard practice for verification of algorithm and equipment for electrochemical impedance measurements*. West Conshohocken, PA, USA: ASTM International.

ASTM G61-86 (2018). *Techniques to assess the corrosion activity of steel reinforced concrete structures*. West Conshohocken, PA, USA: ASTM International.

Bastidas, D. M., Cobo, A., Otero, E., and González, J. A. (2008). Electrochemical rehabilitation methods for reinforced concrete structures: Advantages and pitfalls. *Corros. Eng. Sci. Technol.* 43, 248–255. doi:10.1179/174327808x272423

Bastidas, D. M., Ress, J., Martin, U., Bosch, J., La Iglesia, A., and Bastidas, J. M. (2020). Influencia de la presión de cristalización y variación de volumen durante la formación de herrumbre en ambientes marino y continental-urbano: Factores críticos en la exfoliación. *Rev. Metal. Madr.* 56, e164. doi:10.3989/revmetalm.164

Bauer, H. H. (1968). The electrochemical transfer-coefficient. *J. Electroanal. Chem. Interfacial Electrochem* 16, 419–432. doi:10.1016/s0022-0728(68)80090-7

Bautista, A., Pomares, J. C., González, M. N., and Velasco, F. (2019). Influence of the microstructure of TMT reinforcing bars on their corrosion behavior in concrete with chlorides. *Constr. Build. Mater* 229, 116899. doi:10.1016/j.conbuildmat.2019.116899

Bazant, Z. (1979). Physical model for steel corrosion in concrete sea structures - Theory. *J. Struct. Div.* 105, 1137–1153. doi:10.1061/jsdeag.0005168

Beverskog, B., and Puigdomenech, I. (1996). Revised pourbaix diagrams for iron at 25–300 °C. *Corros. Sci.* 38, 2121–2135. doi:10.1016/s0010-938x(96)00067-4

Brocas, A.-L., Llevot, A., Mantzaridis, C., Cendejas, G., Auvergne, R., Caillol, S., et al. (2014). Epoxidized rosin acids as co-precursors for epoxy resins. *Des. Monomers Polym.* 17, 301–310. doi:10.1080/15685551.2013.840504

Brug, G. J., Van Den Eeden, A. L. G., Sluyters-Rehbach, M., and Sluyters, J. H. (1984). The analysis of electrode impedances complicated by the presence of a constant phase element. *J. Electroanal. Chem. Interfacial Electrochem* 176, 275–295. doi:10.1016/s0022-0728(84)80324-1

Calegari, F., Da Silva, B. C., Tedim, J., Ferreira, M. G. S., Berton, M. A. C., and Marino, C. E. B. (2020). Benzotriazole encapsulation in spray-dried carboxymethylcellulose microspheres for active corrosion protection of carbon steel. *Prog. Org. Coat.* 138, 105329. doi:10.1016/j.porgcoat.2019.105329

Cánovas, M. F., Selv, N. H., and Kawiche, G. M. (1989). Influence on the physical-mechanical properties of portland-cement mortar, have admixtures of colophony and tannin. *Mat. Constr.* 216, 15–22.

Cao, H., Lyu, Z., Dong, W., Zhao, Z., Gan, W., and Wang, Y. (2022). Corrosion experimental research on local damage of epoxy-coated steel bars in concrete under marine environment. *Front. Mater* 8, 616. doi:10.3389/fmats.2021.821716

Dave, R. I., and Shah, N. P. (1997). Effectiveness of ascorbic acid as an oxygen scavenger in improving viability of probiotic bacteria in yoghurts made with commercial starter cultures. *Int. Dairy J.* 7, 435–443. doi:10.1016/s0958-6946(97)00026-5

Dhouibi, L., Triki, E., Salta, M., Rodrigues, P., and Raharinaivo, A. (2003). Studies on corrosion inhibition of steel reinforcement by phosphate and nitrite. *Mat. Struct.* 36, 530–540. doi:10.1617/13893

Ding, S., Serra, C. A., Vandamme, T. F., Yu, W., and Anton, N. (2019). Double emulsions prepared by two-step emulsification: History, state-of-the-art and perspective. *J. Control. Release* 295, 31–49. doi:10.1016/j.jconrel.2018.12.037

Du, W., Yu, J., Gu, S., Wang, R., Li, J., Han, X., et al. (2020). Effect of temperatures on self-healing capabilities of concrete with different shell composition microcapsules containing toluene-di-isocyanate. *Constr. Build. Mater* 247, 118575. doi:10.1016/j.conbuildmat.2020.118575

Gaikwad, K. K., Singh, S., Shin, J., and Lee, Y. S. (2020). Novel polyisoprene based UV-activated oxygen scavenging films and their applications in packaging of beef jerky. *LWT* 117, 108643. doi:10.1016/j.lwt.2019.108643

Geng, S., Hu, J., Yu, J., Zhang, C., Wang, H., and Zhong, X. (2022). Rosin imidazoline as an eco-friendly corrosion inhibitor for the carbon steel in CO_2-containing solution and its synergistic effect with thiourea. *J. Mol. Struct.* 1250, 131778. doi:10.1016/j.molstruc.2021.131778

Giuliani, C., Messina, E., Staccioli, M. P., Pascucci, M., Riccucci, C., Liotta, L. F., et al. (2020). On-demand release of protective agents triggered by environmental stimuli. *Front. Chem.* 8, 304. doi:10.3389/fchem.2020.00304

Jafar, S. A., and Fathi, M. I. (2015). Reducing of corrosion rate in boiler tubes by using oxygen scavengers. *J. Chem. Pet. Eng.* 16, 21–29.

Kenny, A., and Katz, A. (2020). Steel-concrete interface influence on chloride threshold for corrosion – empirical reinforcement to theory. *Constr. Build. Mater* 244, 118376. doi:10.33552/ctcse.2019.04.000586

Keserovic, A., and Birketveit, Ø. (2021). *Crevice corrosion in oxygen scavenger injection system*. London, United Kingdom: SPE Int. Oilfield Corrosion Conf. Exhibit.

Kornyshev, A. A., and Schmickler, W. (1986). On the coverage dependence of the partial charge transfer coefficient. *J. Electroanal. Chem. Interfacial Electrochem* 202, 1–21. doi:10.1016/0022-0728(86)90104-x

Kumar Mehta, P., and Monteiro, P. J. M. (2014). *Concrete: Microstructure, properties, and materials*. Fourth Edition. New York: McGraw-Hill Education.

Lakshmi Priya, S., Chitra, A., Rajendran, S., and Anuradha, K. (2005). Corrosion behaviour of aluminium in rain water containing garlic extract. *Surf. Eng.* 21, 229–231. doi:10.1179/174329405x50073

Macdonald, D. D., Qiu, J., Zhu, Y., Yang, J., Engelhardt, G. R., and Sagüés, A. (2020). Corrosion of rebar in concrete. Part I: Calculation of the corrosion potential in the passive state. *Corros. Sci.* 177, 109018. doi:10.1016/j.corsci.2020.109018

Matsuda, T., Jadhav, N., Kashi, K. B., Jensen, M., and Gelling, V. J. (2019). Release behavior of pH sensitive microcapsules containing corrosion inhibitor. *Prog. Org. Coat.* 132, 9–14. doi:10.1016/j.porgcoat.2019.03.032

Mohamed, A., Visco, D. P., and Bastidas, D. M. (2021). Significance of π–electrons in the design of corrosion inhibitors for carbon steel in simulated concrete pore solution. *Corrosion* 77, 976–990. doi:10.5006/3844

Nong, W., Chen, X., Wang, L., Liang, J., Zhong, L., and Tong, Z. (2013). Thermal decomposition kinetics of abietic acid in static air. *Chin. J. Chem. Eng.* 21, 724–729. doi:10.1016/s1004-9541(13)60493-3

Ostovari, A., Hoseinieh, S. M., Peikari, M., Shadizadeh, S. R., and Hashemi, S. J. (2009). Corrosion inhibition of mild steel in 1M HCl solution by henna extract: A comparative study of the inhibition by henna and its constituents (lawsone, gallic acid, α-d-Glucose and tannic acid). *Corros. Sci.* 51, 1935–1949. doi:10.1016/j.corsci.2009.05.024

Pan, W., Dong, J., Gui, T., Liu, R., Liu, X., and Luo, J. (2022). Fabrication of dual anti-corrosive polyaniline microcapsules via Pickering emulsion for active corrosion protection of steel. *Soft Matter* 18, 2829–2841. doi:10.1039/d2sm00062h

Panda, S., Pattnaik, S., Maharana, L., Botta, G. B., and Mahapatra, A. K. (2013). Design and evaluation of zidovudine loaded natural biodegradable microcapsules employing colophony resin as microencapsulating agent. *Int. J. Pharm. Pharm. Sci.* 5, 799–805.

Rashid, K. H., and Khadom, A. A. (2020). Sodium sulfite as an oxygen scavenger for the corrosion control of mild steel in petroleum refinery wastewater: Optimization, mathematical modeling, surface morphology and reaction kinetics studies. *Reac. Kinet. Mech. Cat.* 129, 1027–1046. doi:10.1007/s11144-020-01738-3

Ren, F., Zheng, Y.-F., Liu, X.-M., Yue, X.-Y., Ma, L., Li, W.-G., et al. (2015). An investigation of the oxidation mechanism of abietic acid using two-dimensional infrared correlation spectroscopy. *J. Mol. Struct.* 1084, 236–243. doi:10.1016/j.molstruc.2014.12.055

Ress, J., Martin, U., Bosch, J., and Bastidas, D. M. (2020). pH-Triggered release of $NaNO_2$ corrosion inhibitors from novel colophony microcapsules in simulated concrete pore solution. *ACS Appl. Mat. Interfaces* 12, 46686–46700. doi:10.1021/acsami.0c13497

Sánchez-Deza, A., Bastidas, D. M., Iglesia, Á. L., Mora, E., and Bastidas, J. M. (2018). Predicción de la vida útil en servicio de edificios de 50 años expuestos a ambientes marinos. *Rev. Metal. Madr.* 54, e111. doi:10.3989/revmetalm.111

Sastri, V. S., and Malaiyandi, M. (1983). Spectral studies on some novel oxygen scavengers and their use in corrosion control of coal slurry pipelines. *Can. Metall. Q.* 22, 241–245. doi:10.1179/cmq.1983.22.2.241

Savéant, J.-M., and Tessier, D. (1982). Variation of the electrochemical transfer coefficient with potential. *Faraday Discuss. Chem. Soc.* 74, 57–72. doi:10.1039/dc9827400057

Schremp, F. W., Chittum, J. F., and Arczynski, T. S. (1961). Use of oxygen scavengers to control external corrosion of oil-string casing. *J. Pet. Technol.* 13, 703–711. doi:10.2118/1606-g

Scrivenand, B., and Winter, T. R. (1978). Chemical oxygen scavengers: Use of hydrazine and tannins for boiler water treatment. *Anti-Corrosion Meth. Material* 25, 10–11. doi:10.1108/eb007075

Yan, M., Vetter, C. A., and Gelling, V. J. (2013). Corrosion inhibition performance of polypyrrole Al flake composite coatings for Al alloys. *Corros. Sci.* 70, 37–45. doi:10.1016/j.corsci.2012.12.019

Zhang, Y., Yu, M., Chen, C., Li, S., and Liu, J. (2022). Self-healing coatings based on stimuli-responsive release of corrosion inhibitors: A review. *Front. Mater* 8.

Zheng, X., Yang, S., and Sun, S. (2020). Determination of the corrosion rate of steel bars in concrete based on the porosity of interfacial zone. *Front. Mater* 7, 339. doi:10.3389/fmats.2020.573193